

Dynamic Nuclear Polarization of Metal–Organic Frameworks Using Photoexcited Triplet Electrons

Saiya Fujiwara,^{†,§} Masanori Hosoyamada,^{†,§} Kenichiro Tateishi,^{*,‡,‡,‡,‡,‡} Tomohiro Uesaka,^{‡,‡,‡,‡,‡} Keiko Ideta,^{||} Nobuo Kimizuka,^{*,†,‡} and Nobuhiro Yanai^{*,†,‡,‡,‡,‡}

[†]Department of Chemistry and Biochemistry, Graduate School of Engineering, Center for Molecular Systems (CMS), Kyushu University, 744 Moto-oka, Nishi-ku, Fukuoka 819-0395, Japan

[‡]Cluster for Pioneering Research, RIKEN, 2-1 Hirosawa, Wako, Saitama 351-0198, Japan

[#]Nishina Center for Accelerator-Based Science, RIKEN, 2-1 Hirosawa, Wako, Saitama 351-0198, Japan

^{||}Institute for Materials Chemistry and Engineering, Kyushu University, 6-1 Kasuga-koen, Kasuga, Fukuoka 816-8580, Japan

[¶]PRESTO, JST, Honcho 4-1-8, Kawaguchi, Saitama 332-0012, Japan

Supporting Information

ABSTRACT: While dynamic nuclear polarization based on photoexcited triplet electrons (triplet-DNP) has the potential to hyperpolarize nuclear spins of target substrates in the low magnetic field at room temperature, there has been no triplet-DNP system offering structural rigidity and substrate accessibility. Here, we report the first example of triplet-DNP of nanoporous metal–organic frameworks. Accommodation of a carboxylate-modified pentacene derivative in a partially deuterated ZIF-8 (D-ZIF-8) results in a clear ¹H NMR signal enhancement over thermal equilibrium.

Nuclear magnetic resonance (NMR) spectroscopy and magnetic resonance imaging (MRI) are versatile methods in modern chemistry and biology fields. Nevertheless, they suffer from intrinsically limited sensitivity due to the low nuclear spin polarization at ambient temperature. One of the promising methods to overcome this limitation is dynamic nuclear polarization (DNP), which enhances nuclear polarization by transferring spin polarization from electrons to nuclei.^{1,2} The application of DNP has opened up new possibilities, in particular for molecular imaging with MRI. For example, the use of DNP enables tumor imaging by monitoring hyperpolarized metabolic small molecules, which is currently under clinical trial.^{3–6} While significant polarization enhancement (ϵ) has been achieved by using paramagnetic radical compounds as the polarizing agents,^{7–9} the use of cryogenic temperatures around 1 K inevitably increases the cost of the instruments and makes it difficult to polarize fragile biological substances.

The solution to this issue has been proposed by employing nonthermal electron polarization in photoexcited triplet state at room temperature.^{10–15} In the typical scheme of DNP based on a photoexcited triplet (triplet-DNP, Figure 1a), spin-selective intersystem crossing (ISC) produces a large electron spin polarization in the excited triplet state sublevels regardless of temperature,¹⁶ and this polarization is effectively transferred to nuclear spins by the integrated solid effect (ISE).^{17,18} Following its first report,¹⁰ room-temperature triplet-DNP has

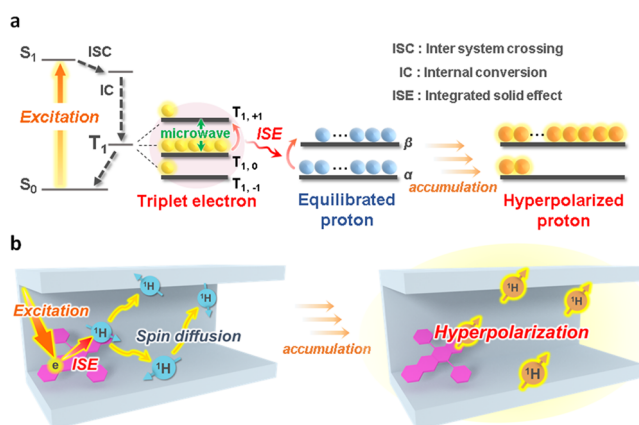


Figure 1. (a) Typical scheme of triplet-DNP. Photoexcitation of the polarizing agent is followed by spin-selective intersystem crossing (ISC). The resulting large electron spin polarization is transferred to the nuclear spin polarization through the integrated solid effect (ISE). (b) Schematic illustration of triplet-DNP in MOFs accommodating polarizing agents.

provided high enhancements in organic crystals such as *p*-terphenyl with long spin–lattice relaxation time (T_1).^{10–12,14} However, it remains difficult for such organic crystals to accommodate target molecules to be monitored. While amorphous solids such as *o*-terphenyl were employed as host matrices to accommodate target substrates, the flexible structure requires the cooling of the sample for triplet-DNP (~ 120 K).¹³ Therefore, despite these efforts, it remains a grand challenge to develop a room-temperature triplet-DNP system with accessibility for polarizing targets. While pioneering works employed porous materials for low-temperature radical-based DNP to accommodate target molecules,^{19–24} there have been no examples of room-temperature DNP using porous matrices.

In this work, we show the first example of employing metal–organic frameworks (MOFs)^{25–33} as host materials for triplet-DNP (Figure 1b). MOFs offer not only rigid crystalline

Received: September 18, 2018

structures but also nanopores for guest accommodation. For the proof-of-concept, it is necessary to satisfy the following conditions: (i) high dispersibility of polarizing agent in MOFs; (ii) long ^1H T_1 of MOFs. Based on our previous work using a soluble pentacene derivative (6, 13-diphenylpentacene (DPP)) for triplet-DNP,³⁴ we modified the typical polarizing agent pentacene with metal-coordinating carboxylate moieties (4,4'-(pentacene-6,13-diyl)dibenzoic acid (PDBA)), Figure 2a) for

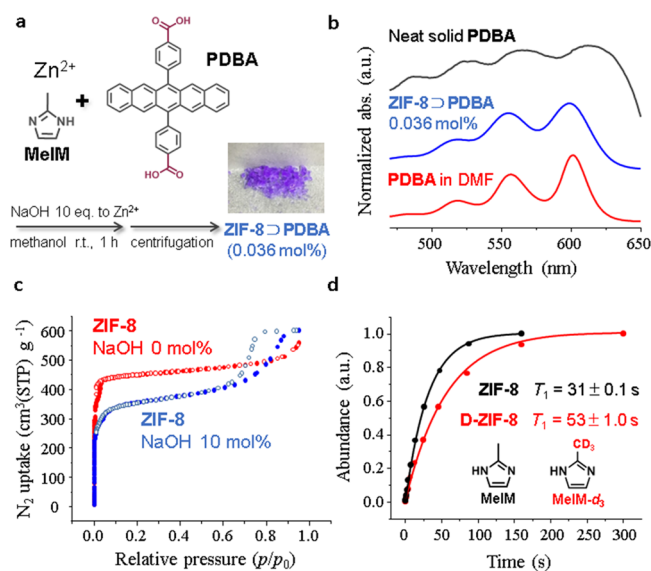


Figure 2. (a) Synthetic scheme and a photograph of ZIF-8 \supset PDBA. (b) Absorption spectra of a DMF solution of PDBA (50 μM , red), ZIF-8 \supset PDBA (0.036 mol %, blue), and neat solid PDBA (black). (c) N_2 adsorption (filled circles) and desorption (open circles) isotherms at 77 K for ZIF-8 synthesized in the absence (red) and presence (blue) of 10 mol % NaOH. (d) ^1H spin–lattice relaxation (T_1) data of ZIF-8 (black) and D-ZIF-8 (red) acquired with the saturation–recovery sequence.

its introduction into MOFs. A relatively long ^1H T_1 has been reported for a prototypical diamagnetic Zn^{2+} -based MOF, $[\text{Zn}(\text{MeIM})_2]_n$ (ZIF-8; MeIM = 2-methylimidazole).^{35–39} A partial deuteration of MeIM ligands allows the elongation of T_1 of partially deuterated D-ZIF-8. Polarization transfer from PDBA triplet electrons to ^1H nuclei in D-ZIF-8 resulted in a clear enhancement ($\epsilon = 58$) of ^1H NMR signals of D-ZIF-8 at a low magnetic field of 0.67 T and room temperature.

We synthesized the new pentacene derivative PDBA starting from 6,13-pentacenequinone (Scheme S1, Supporting Information). The PDBA molecules were successfully accommodated during the crystallization of ZIF-8 in methanol in the presence of NaOH at room temperature (Figure 2a). It has been reported that the aggregation of pentacene decreases the effect of triplet-DNP.¹² To gain insights into the dispersibility of PDBA in ZIF-8, we measured absorption spectra. A dimethylformamide (DMF) solution of PDBA ($[\text{PDBA}] = 50 \mu\text{M}$) exhibited structured π – π^* absorption bands at 601.5, 557, and 518.5 nm (Figure 2b). The absorption bands in the neat solid PDBA showed red-shifts to 616, 565.5, and 528 nm and broadening due to intermolecular interactions among aggregated PDBA. Interestingly, the absorption peak positions of PDBA in ZIF-8 depend on the NaOH concentration and became almost identical to those in solution in the presence of 10 mol % NaOH compared with Zn(II) ions (Figures 2b, S3, Supporting Information). The enhanced nucleation and

growth rate of ZIF-8 crystallization by the base addition might kinetically trap PDBA molecules inside ZIF-8 before aggregation of PDBA.

The dispersed accommodation of PDBA in ZIF-8 is further supported by fluorescence studies. Time-resolved fluorescence measurements of PDBA in DMF ($[\text{PDBA}] = 50 \mu\text{M}$) showed a single-exponential decay with a lifetime of 7.8 ns (Figure S4b, Supporting Information). No detectable fluorescence was observed from bulk PDBA solids, probably due to the fluorescence quenching by singlet fission among aggregated PDBA molecules.⁴⁰ On the other hand, ZIF-8 \supset PDBA clearly showed fluorescence bands similar to those of the DMF solution (Figure S4a, Supporting Information). The fluorescence decay of ZIF-8 \supset PDBA could be fitted with three components (2.0 ns (6.3%), 6.1 ns (56%), and 12.8 ns (37%), Figure S4b, Supporting Information), which may reflect the partial aggregation of PDBA molecules.

The included amount of PDBA inside ZIF-8 was quantified from the UV–vis absorbance after digesting the composite with HCl in methanol. The inclusion amount can be controlled by changing the concentration of PDBA and NaOH (Figure S5, Supporting Information). The included amount of PDBA increased by increasing the NaOH concentration. As a control experiment, no uptake of nonionic DPP into ZIF-8 was observed, suggesting the accommodation of PDBA through coordination of carboxylate moieties to Zn^{2+} ions of ZIF-8. With reference to previously optimized systems including 0.01–0.05 mol % of pentacene in dense *p*-terphenyl crystals,^{12,13} we prepared ZIF-8 samples containing 0.036 mol % of PDBA.

The structure of ZIF-8 synthesized in the presence of NaOH (10 mol % of Zn^{2+} ions) was confirmed by scanning electron microscopy (SEM), elemental analysis, powder X-ray diffraction (PXRD), and N_2 adsorption measurements. SEM images showed that the addition of NaOH decreased the crystal size from ca. 30 nm to 10 nm (Figure S6, Supporting Information). This is in good agreement with previous reports about the effect of the base upon crystallization of ZIF-8.^{41,42} The smaller crystal size of ZIF-8 by base addition was explained by faster nucleation and growth of ZIF-8 due to the enhanced deprotonation of MeIM ligands. The presence of NaOH did not affect the phase purity of ZIF-8, as confirmed by elemental analysis and PXRD patterns (Figure S7, Supporting Information). PXRD patterns showed peak broadening by the addition of NaOH, which agrees with the reduced crystal size. The N_2 adsorption isotherms for both ZIF-8 samples with/without NaOH showed N_2 uptake in the low-pressure region ($P/P_0 < 0.1$), characteristic of microporous materials (Figure 2c). The BET surface area of ZIF-8 was mostly maintained when NaOH was used (1280 $\text{m}^2 \text{g}^{-1}$) compared with that of the pristine ZIF-8 (1680 $\text{m}^2 \text{g}^{-1}$). Only ZIF-8 synthesized with NaOH showed an additional N_2 absorption in the middle-pressure region ($P/P_0 > 0.6$) and a hysteresis in the desorption process. This behavior is typical for mesoporous materials, and the observed mesopores are ascribed to the grain boundaries between ZIF-8 nanoparticles. These PXRD and gas adsorption results agree well with the previous reports of ZIF-8 nanocrystals.^{41,42}

In practice, the spin–lattice relaxation time (T_1) is the major factor in determining the attainable spin polarization since the polarization accumulation competes with the spin–lattice relaxation. To obtain the ^1H T_1 value, we carried out solid-state magic angle spinning (MAS)-NMR measurements of

ZIF-8 at room temperature (Figure S8a, Supporting Information). Samples were packed in an Ar-filled glovebox to exclude the relaxation effect by paramagnetic oxygen molecules. The ^1H T_1 value of ZIF-8 was estimated as 31 ± 0.1 s (Figure 2d).³⁹ We confirmed that the inclusion of 0.036 mol % of PDBA did not significantly affect the ^1H T_1 value of ZIF-8 (25 ± 0.1 s, Figure S8b, Supporting Information). To further increase the ^1H T_1 value, we synthesized a partially deuterated MOF. For spin-1/2 systems, spin–lattice relaxation is mainly caused by fluctuating local magnetic fields at the site of nuclear spins due to the thermal motion of molecules.⁴³ Generally, in solids, every spin is densely coupled to other spins and the T_1 values are averaged out over whole protons. Accordingly, we assumed that the rotation of methyl groups in ZIF-8 decreases the ^1H T_1 value and synthesized a partially deuterated ligand, MeIM- d_3 (Figure 2d, Scheme S2, SI), to construct methyl-deuterated ZIF-8 (denoted as D-ZIF-8). As expected, a longer ^1H T_1 value of 53 ± 1.0 s was successfully obtained for D-ZIF-8 (Figures 2d, S8c, Supporting Information). In the following experiments, D-ZIF-8 \supset PDBA containing 0.036 mol % of PDBA was used.

The generation of electron spin polarization in photoexcited triplet state was investigated by time-resolved electron spin resonance (ESR) measurements at room temperature. Under pulsed laser irradiation at 589 nm, the ESR spectrum of D-ZIF-8 \supset PDBA showed a characteristic line shape of spin-polarized triplet state at room temperature, in which the $T_{1,0}$ triplet sublevel is populated preferentially and $\Delta m = 1$ $T_{1,0} \rightarrow T_{1,-1}$ and $T_{1,0} \rightarrow T_{1,+1}$ transitions were observed as emission at 305 mT and absorption at 355 mT, respectively (Figure 3a). The

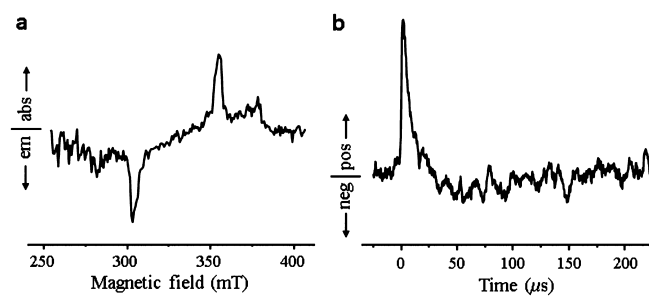


Figure 3. (a) Time-resolved ESR spectrum of D-ZIF-8 \supset PDBA at room temperature just after photoexcitation at 589 nm. (b) Decay of the ESR peak at 355 mT under pulsed photoexcitation at 589 nm.

signal intensity of the peak at 355 mT showed microsecond-scale decay profiles characteristic of the triplet excited state (Figure 3b). The negative components derived from $T_{1,-1} \rightarrow S_0/T_{1,+1} \rightarrow S_0$ transitions were also observed at around 50 μs , supporting the spin-selective ISC.^{44,45}

The transfer of spin polarization from photoexcited triplet electrons to ^1H nuclei was evaluated by comparing the ^1H NMR signal with and without the triplet-DNP process at 0.67 T and room temperature (see Supporting Information for detailed measurement setup). PDBA molecules were photoexcited by a pulsed 589 nm laser (500 Hz), followed by microwave irradiation (18.1 GHz) and field sweep (± 100 G) for polarization transfer (ISE sequence, Figure 4a). The duration of microwave irradiation (10 μs) was optimized based on the enhancement of the ^1H NMR signal intensity. The extra time of 2 ms was employed to avoid the sample degradation.

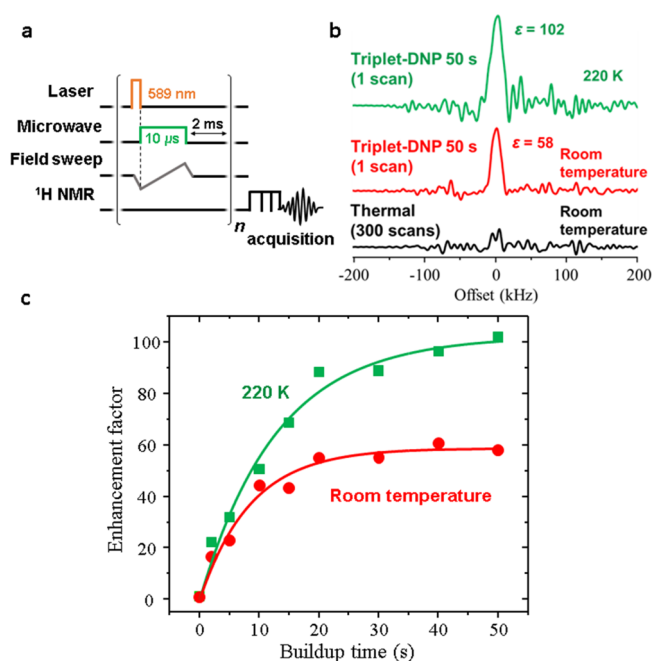


Figure 4. (a) Sequence of the triplet-DNP process. (b) ^1H NMR signals of D-ZIF-8 \supset PDBA under thermal conditions (300 scans every 3 min) and after triplet-DNP (ISE sequence for 50 s and 1 scan) at room temperature and 220 K. (c) ^1H polarization buildup curve of D-ZIF-8 \supset PDBA at room temperature and 220 K. The enhancement factors were calculated by comparing the peak area after triplet-DNP with that of thermal equilibrium at room temperature.

After repeating this process to accumulate the spin polarization, ^1H NMR spectra were immediately measured. Because the accumulation of spin polarization by ISE competes with spin–lattice relaxation, the ^1H spin polarization becomes saturated by elongating the triplet-DNP process (Figure 4c). The ^1H NMR signal intensity of D-ZIF-8 \supset PDBA showed a large enhancement factor of 58, and the signal-to-noise ratio of ^1H NMR spectra was significantly improved by the triplet-DNP process (Figure 4b). Besides, we investigated the triplet-DNP process at a lower temperature (220 K), which is relevant to adsorption of the ^{129}Xe gas probe.^{46,47} As a result, 85 and 102 times enhancement were achieved compared to the thermal equilibrium at 220 K and room temperature, respectively. The change in the noise level of the NMR signal by reducing the temperature is mainly attributed to the thermal controller. The polarization buildup curve was fit to $A[1 - \exp(-t/T_B)]$, giving a buildup constant T_B of 13 s at 220 K, which was increased relative to room temperature (8.5 s). This indicates that the increase in the ^1H NMR signal enhancement at low temperature is mainly due to the reduced molecular mobility and prolonged ^1H T_1 . We note that D-ZIF-8 \supset PDBA was unstable in repeated long-term laser irradiation, which would be solved by improving the dispersibility and chemical stability of the polarizing agent.

In conclusion, we demonstrate the first spin hyperpolarization of MOF protons based on triplet-DNP. The selective deuteration of the framework effectively suppressed the spin relaxation, giving a long ^1H T_1 value over 50 s. The newly synthesized polarizing agent PDBA allowed the generation of electron spin polarization by photoexcitation in D-ZIF-8. As a result, by applying triplet-DNP, the significant ^1H NMR signal enhancement factor (ϵ) of 58 was achieved at room

temperature. A further increase of the polarization enhancement factor would be achieved by improving the dispersibility and chemical stability of the polarizing agent and by elongating the MOF T_1 . This work proves the concept of using MOFs as “porous” and “rigid” hosts for triplet-DNP, and the polarization transfer to various guest target molecules is the obvious next step. This work provides an important initial step toward hyperpolarizing various molecules of interest in chemistry, physics, and biology at room temperature.

■ ASSOCIATED CONTENT

● Supporting Information

The Supporting Information is available free of charge on the ACS Publications website at DOI: 10.1021/jacs.8b10121.

Experimental details, NMR spectra, UV–vis absorption spectra, fluorescence spectra, fluorescence decays, SEM images, PXRD patterns (PDF)

■ AUTHOR INFORMATION

Corresponding Authors

*kenichiro.tateishi@riken.jp

*n-kimi@mail.cstm.kyushu-u.ac.jp

*yanai@mail.cstm.kyushu-u.ac.jp

ORCID

Kenichiro Tateishi: 0000-0001-5566-526X

Nobuo Kimizuka: 0000-0001-8527-151X

Nobuhiro Yanai: 0000-0003-0297-6544

Author Contributions

[§]S. Fujiwara and M. Hosoyamada contributed equally.

Notes

The authors declare no competing financial interest.

■ ACKNOWLEDGMENTS

This work was partly supported by JSPS KAKENHI grant numbers JP25220805, JP17H04799, and JP16H06513 and the Tobe Maki Scholarship Foundation. K.T. acknowledges partial support from the RIKEN Pioneering Project “Dynamic Structural Biology”.

■ REFERENCES

- (1) Carver, T. R.; Slichter, C. P. Polarization of Nuclear Spins in Metals. *Phys. Rev.* **1953**, *92*, 212–213.
- (2) Overhauser, A. W. Polarization of Nuclei in Metals. *Phys. Rev.* **1953**, *92*, 411–415.
- (3) Golman, K.; Zandt, R. I.; Lerche, M.; Pehrson, R.; Ardenkjær-Larsen, J. H. Metabolic Imaging by Hyperpolarized ¹³C Magnetic Resonance Imaging for *In vivo* Tumor Diagnosis. *Cancer Res.* **2006**, *66*, 10855–10860.
- (4) Gallagher, F. A.; Kettunen, M. I.; Day, S. E.; Hu, D.-E.; Ardenkjær-Larsen, J. H.; Zandt, R. I.; Jensen, P. R.; Karlsson, M.; Golman, K.; Lerche, M. H.; Brindle, K. M. Magnetic resonance imaging of pH *in vivo* using hyperpolarized ¹³C-labelled bicarbonate. *Nature* **2008**, *453*, 940–943.
- (5) Keshari, K. R.; Wilson, D. M. Chemistry and biochemistry of ¹³C hyperpolarized magnetic resonance using dynamic nuclear polarization. *Chem. Soc. Rev.* **2014**, *43*, 1627–1659.
- (6) Siddiqui, S.; Kadlecsek, S.; Pourfathi, M.; Xin, Y.; Mannherz, W.; Hamedani, H.; Drachman, N.; Ruppert, K.; Clapp, J.; Rizi, R. The use of hyperpolarized carbon-13 magnetic resonance for molecular imaging. *Adv. Drug Delivery Rev.* **2017**, *113*, 3–23.
- (7) Ardenkjær-Larsen, J. H.; Fridlund, B.; Gram, A.; Hansson, G.; Hansson, L.; Lerche, M. H.; Servin, R.; Thanning, M.; Golman, K.

Increase in signal-to-noise ratio of > 10,000 times in liquid-state NMR. *Proc. Natl. Acad. Sci. U. S. A.* **2003**, *100*, 10158–10163.

(8) Song, C.; Hu, K.-N.; Joo, C.-G.; Swager, T. M.; Griffin, R. G. TOTAPOL: A Biradical Polarizing Agent for Dynamic Nuclear Polarization Experiments in Aqueous Media. *J. Am. Chem. Soc.* **2006**, *128*, 11385–11390.

(9) Ardenkjær-Larsen, J. H. On the present and future of dissolution-DNP. *J. Magn. Reson.* **2016**, *264*, 3–12.

(10) Henstra, A.; Lin, T.-S.; Schmidt, J.; Wenckebach, W. Th. HIGH DYNAMIC NUCLEAR POLARIZATION AT ROOM TEMPERATURE. *Chem. Phys. Lett.* **1990**, *165*, 6–10.

(11) Iinuma, M.; Takahashi, Y.; Shake, I.; Oda, M.; Masaike, A.; Yabuzaki, T.; Shimizu, H. M. Proton polarization with *p*-terphenyl crystal by integrated solid effect on photoexcited triplet state. *J. Magn. Reson.* **2005**, *175*, 235–241.

(12) Takeda, K. *Triplet State Dynamic Nuclear Polarization*; VDM Verlag Dr. Müller: Saarbrücken, Germany, 2009.

(13) Tateishi, K.; Negoro, M.; Kagawa, A.; Kitagawa, M. Dynamic Nuclear Polarization with Photoexcited Triplet Electrons in a Glassy Matrix. *Angew. Chem., Int. Ed.* **2013**, *52*, 13307–13310.

(14) Tateishi, K.; Negoro, M.; Nishida, S.; Kagawa, A.; Morita, Y.; Kitagawa, M. Room temperature hyperpolarization of nuclear spins in bulk. *Proc. Natl. Acad. Sci. U. S. A.* **2014**, *111*, 7527–7530.

(15) Eichhorn, T. R.; Niketic, N.; van den Brandt, B.; Filges, U.; Panzner, T.; Rantsiou, E.; Wenckebach, W. Th.; Hautle, P. Proton polarization above 70% by DNP using photo-excited triplet states, a first step towards a broadband neutron spin filter. *Nucl. Instrum. Methods Phys. Res., Sect. A* **2014**, *754*, 10–14.

(16) Sloop, D. J.; Yu, H.-L.; Lin, T.-S.; Weissman, S. I. Electron spin echoes of a photoexcited triplet: Pentacene in *p*-terphenyl crystals. *J. Chem. Phys.* **1981**, *75*, 3746–3757.

(17) Henstra, A.; Wenckebach, W. Th. Dynamic nuclear polarisation via the integrated solid effect I: theory. *Mol. Phys.* **2014**, *112*, 1761–1772.

(18) Can, T. V.; Weber, R. T.; Walsh, J. J.; Swager, T. M.; Griffin, R. G. Frequency-Swept Integrated Solid Effect. *Angew. Chem.* **2017**, *129*, 6848–6852.

(19) Lesage, A.; Lelli, M.; Gajan, D.; Caporini, M. A.; Vitzthum, V.; Miéville, P.; Alauzun, J.; Roussey, A.; Thieuleux, C.; Mehdi, A.; Bodenhausen, G.; Copéret, C.; Emsley, L. Surface Enhanced NMR Spectroscopy by Dynamic Nuclear Polarization. *J. Am. Chem. Soc.* **2010**, *132*, 15459–15461.

(20) Lafon, O.; Rosay, M.; Aussenac, F.; Lu, X.; Trébosc, J.; Cristini, O.; Kinowski, C.; Touati, N.; Vezin, H.; Amoureux, J.-P. Beyond the silica surface by direct silicon-29 dynamic nuclear polarization. *Angew. Chem., Int. Ed.* **2011**, *50*, 8367–8370.

(21) Rossini, A. J.; Zagdoun, A.; Lelli, M.; Lesage, A.; Copéret, C.; Emsley, L. Dynamic Nuclear Polarization Surface Enhanced NMR Spectroscopy. *Acc. Chem. Res.* **2013**, *46*, 1942–1951.

(22) Gajan, D.; Bornet, A.; Vuichoud, B.; Milani, J.; Melzi, R.; van Kalker, H. A.; Veyre, L.; Thieuleux, C.; Conley, M. P.; Gruning, W. R.; Schwarzwalder, M.; Lesage, A.; Copéret, C.; Bodenhausen, G.; Emsley, L.; Jannin, S. Hybrid polarizing solids for pure hyperpolarized liquids through dissolution dynamic nuclear polarization. *Proc. Natl. Acad. Sci. U. S. A.* **2014**, *111*, 14693–14697.

(23) Vuichoud, B.; Canet, E.; Milani, J.; Bornet, A.; Baudouin, D.; Veyre, L.; Gajan, D.; Emsley, L.; Lesage, A.; Copéret, C.; Thieuleux, C.; Bodenhausen, G.; Koptuyug, I.; Jannin, S. Hyperpolarization of Frozen Hydrocarbon Gases by Dynamic Nuclear Polarization at 1.2 K. *J. Phys. Chem. Lett.* **2016**, *7*, 3235–3239.

(24) Cao, W.; Wang, W. D.; Xu, H. S.; Sergeev, I. V.; Struppe, J.; Wang, X.; Mentink-Vigier, F.; Gan, Z.; Xiao, M.-X.; Wang, L.-Y.; Chen, G.-P.; Ding, S.-Y.; Bai, S.; Wang, W. Exploring Applications of Covalent Organic Frameworks: Homogeneous Reticulation of Radicals for Dynamic Nuclear Polarization. *J. Am. Chem. Soc.* **2018**, *140*, 6969–6977.

(25) Yaghi, O. M.; O’Keeffe, M.; Ockwig, N. W.; Chae, H. K.; Eddaoudi, M.; Kim, J. Reticular synthesis and the design of new materials. *Nature* **2003**, *423*, 705–714.

- (26) Kitagawa, S.; Kitaura, R.; Noro, S. Functional Porous Coordination Polymers. *Angew. Chem., Int. Ed.* **2004**, *43*, 2334–2375.
- (27) Inokuma, Y.; Kawano, M.; Fujita, M. Crystalline molecular flasks. *Nat. Chem.* **2011**, *3*, 349–358.
- (28) Sumida, K.; Rogow, D. L.; Mason, J. A.; McDonald, T. M.; Bloch, E. D.; Herm, Z. R.; Bae, T.-H.; Long, J. R. Carbon Dioxide Capture in Metal-Organic Frameworks. *Chem. Rev.* **2012**, *112*, 724–781.
- (29) Ramaswamy, P.; Wong, N. E.; Shimizu, G. K. MOFs as proton conductors - challenges and opportunities. *Chem. Soc. Rev.* **2014**, *43*, 5913–5932.
- (30) So, M. C.; Wiederrecht, G. P.; Mondloch, J. E.; Hupp, J. T.; Farha, O. K. Metal-organic framework materials for light-harvesting and energy transfer. *Chem. Commun.* **2015**, *51*, 3501–3510.
- (31) Sun, L.; Campbell, M. G.; Dincă, M. Electrically Conductive Porous Metal-Organic Frameworks. *Angew. Chem., Int. Ed.* **2016**, *55*, 3566–3579.
- (32) Férey, G.; Serre, C. Large breathing effects in three-dimensional porous hybrid matter: facts, analyses, rules and consequences. *Chem. Soc. Rev.* **2009**, *38*, 1380–1399.
- (33) Li, J. R.; Sculley, J.; Zhou, H.-C. Metal-Organic Frameworks for Separations. *Chem. Rev.* **2012**, *112*, 869–932.
- (34) Tateishi, K.; Uesaka, T.; Negoro, M.; Kitagawa, M. Nuclear spin polarization enhancing method through dynamic nuclear polarization by using soluble pentacene. Patent WO2017002761A1, Jan 5, 2017.
- (35) Huang, X.-C.; Lin, Y. Y.; Zhang, J.-P.; Chen, X.-M. Ligand-Directed Strategy for Zeolite-Type Metal-Organic Frameworks: Zinc(II) Imidazolates with Unusual Zeolitic Topologies. *Angew. Chem., Int. Ed.* **2006**, *45*, 1557–1559.
- (36) Park, K. S.; Ni, Z.; Côté, A. P.; Choi, J. Y.; Huang, R.; Uribe-Romo, F. J.; Chae, H. K.; O’Keeffe, M.; Yaghi, O. M. Exceptional chemical and thermal stability of zeolitic imidazolate frameworks. *Proc. Natl. Acad. Sci. U. S. A.* **2006**, *103*, 10186–10191.
- (37) Cravillon, J.; Münzer, S.; Lohmeier, S.-J.; Feldhoff, A.; Huber, K.; Wiebcke, M. Rapid Room-Temperature Synthesis and Characterization of Nanocrystals of a Prototypical Zeolitic Imidazolate Framework. *Chem. Mater.* **2009**, *21*, 1410–1412.
- (38) Lu, G.; Li, S.; Guo, Z.; Farha, O. K.; Hauser, B. G.; Qi, X.; Wang, Y.; Wang, X.; Han, S.; Liu, X.; DuChene, J. S.; Zhang, H.; Zhang, Q.; Chen, X.; Ma, J.; Loo, S. C.; Wei, W. D.; Yang, Y.; Hupp, J. T.; Huo, F. Imparting functionality to a metal-organic framework material by controlled nanoparticle encapsulation. *Nat. Chem.* **2012**, *4*, 310–316.
- (39) Morris, W.; Stevens, C. J.; Taylor, R. E.; Dybowski, C.; Yaghi, O. M.; Garcia-Garibay, M. A. NMR and X-ray Study Revealing the Rigidity of Zeolitic Imidazolate Frameworks. *J. Phys. Chem. C* **2012**, *116*, 13307–13312.
- (40) Bakulin, A. A.; Morgan, S. E.; Kehoe, T. B.; Wilson, M. W.; Chin, A. W.; Zigmantas, D.; Egorova, D.; Rao, A. Real-time observation of multiexcitonic states in ultrafast singlet fission using coherent 2D electronic spectroscopy. *Nat. Chem.* **2016**, *8*, 16–23.
- (41) Cravillon, J.; Nayuk, R.; Springer, S.; Feldhoff, A.; Huber, K.; Wiebcke, M. Controlling Zeolitic Imidazolate Framework Nano- and Microcrystal Formation: Insight into Crystal Growth by Time-Resolved In Situ Static Light Scattering. *Chem. Mater.* **2011**, *23*, 2130–2141.
- (42) Zhang, C.; Gee, J. A.; Sholl, D. S.; Lively, R. P. Crystal-Size-Dependent Structural Transitions in Nanoporous Crystals: Adsorption-Induced Transitions in ZIF-8. *J. Phys. Chem. C* **2014**, *118*, 20727–20733.
- (43) Levitt, M. H. *Spin Dynamics: Basics of Nuclear Magnetic Resonance*. 2nd ed.; John Wiley & Sons Ltd: The Atrium, Southern Gate, Chichester, 2008.
- (44) Terazima, M.; Yamauchi, S.; Hirota, N. Properties of the short-lived triplet states of pyridazine and 3,6-dichloropyridazine studied by a time-resolved EPR method. *J. Chem. Phys.* **1986**, *84*, 3679–3687.
- (45) Hirota, N.; Yamauchi, S. Short-lived excited triplet states studied by time-resolved EPR spectroscopy. *J. Photochem. Photobiol., C* **2003**, *4*, 109–124.
- (46) Mugler, J. P., 3rd; Altes, T. A.; Ruset, I. C.; Dregely, I. M.; Mata, J. F.; Miller, G. W.; Ketel, S.; Ketel, J.; Hersman, F. W.; Ruppert, K. Simultaneous magnetic resonance imaging of ventilation distribution and gas uptake in the human lung using hyperpolarized xenon-129. *Proc. Natl. Acad. Sci. U. S. A.* **2010**, *107*, 21707–21712.
- (47) Shapiro, M. G.; Ramirez, R. M.; Sperling, L. J.; Sun, G.; Sun, J.; Pines, A.; Schaffer, D. V.; Bajaj, V. S. Genetically encoded reporters for hyperpolarized xenon magnetic resonance imaging. *Nat. Chem.* **2014**, *6*, 629–634.